The fluid dynamics of canine olfaction: unique nasal airflow patterns as an explanation of macrosmia

Brent A. Craven[1,2,*], Eric G. Paterson[1] and Gary S. Settles[2]

[1]*Applied Research Laboratory, and* [2]*Gas Dynamics Laboratory, Department of Mechanical and Nuclear Engineering, The Pennsylvania State University, University Park, PA 16802, USA*

The canine nasal cavity contains hundreds of millions of sensory neurons, located in the olfactory epithelium that lines convoluted nasal turbinates recessed in the rear of the nose. Traditional explanations for canine olfactory acuity, which include large sensory organ size and receptor gene repertoire, overlook the fluid dynamics of odorant transport during sniffing. But odorant transport to the sensory part of the nose is the first critical step in olfaction. Here we report new experimental data on canine sniffing and demonstrate allometric scaling of sniff frequency, inspiratory airflow rate and tidal volume with body mass. Next, a computational fluid dynamics simulation of airflow in an anatomically accurate three-dimensional model of the canine nasal cavity, reconstructed from high-resolution magnetic resonance imaging scans, reveals that, during sniffing, spatially separate odour samples are acquired by each nostril that may be used for bilateral stimulus intensity comparison and odour source localization. Inside the nose, the computation shows that a unique nasal airflow pattern develops during sniffing, which is optimized for odorant transport to the olfactory part of the nose. These results contrast sharply with nasal airflow in the human. We propose that mammalian olfactory function and acuity may largely depend on odorant transport by nasal airflow patterns resulting from either the presence of a highly developed olfactory recess (in macrosmats such as the canine) or the lack of one (in microsmats including humans).

Keywords: canine olfaction; macrosmatic; olfactory acuity;
nasal airway; sniff; computational fluid dynamics

1. INTRODUCTION

The olfactory acuity of the dog (*Canis familiaris*), which can detect odorant concentration levels at $1-2$ parts per trillion, is roughly $10\,000-100\,000$ times that of the human (Walker *et al.* 2003, 2006). Though olfactory organ size (Smith *et al.* 2004; Pihstrom *et al.* 2005), neuronal density (Quignon *et al.* 2003) and the number of functional genes versus pseudogenes in the olfactory receptor gene family (Rouquier *et al.* 1998, 2000; Shepherd 2004; Rouquier & Giorgi 2007) certainly contribute to this disparity, these measures nonetheless fail to consider the anatomical structure of the nasal cavity and odorant transport from the external environment, by sniffing, to receptors on the cilia of the olfactory epithelium.

In a comparison of many species, Negus (1958) first recognized that gross anatomical structure of the nasal cavity is an indicator of olfactory acuity, with most keen-scented (macrosmatic) animals possessing a common nasal architecture that is absent in feeble-scented (microsmatic) species. Generally, the olfactory mucosa of macrosmats (e.g. dog (Evans 1993; Craven

et al. 2007), cat (Negus 1958), rabbit (Kuramoto *et al.* 1985) and rat (Schreider & Raabe 1981)) is relegated to an 'olfactory recess', located in the rear of the nasal cavity and excluded from the main respiratory airflow path by a bony plate, the *lamina transversa* (figures 1 and 2*a*; Craven *et al.* 2007). The olfactory recess 'is seen at its height of perfection in the dog' (Negus 1958), but, as shown in figure 2*b*, is largely absent in microsmatic primates, specifically the Haplorrhini suborder (Smith *et al.* 2004, 2007) (e.g. human (Hornung 2006), rhesus monkey (Schreider & Raabe 1981) and marmoset (Smith *et al.* 2004)). In these species, the olfactory mucosa is characteristically located in the superior part of the nasal cavity, near the 'roof' of the 'main nasal passage' (figure 2*b*; Proctor 1982; Morrison & Costanzo 1990; Smith *et al.* 2007).

Despite the apparent correlation between nasal cavity structure and mammalian olfactory acuity, a suitable physical explanation has not yet been given, though few studies have considered the role of intranasal fluid dynamics and odorant transport. The fluid dynamics of olfaction includes odorant collection via active sniffing (external aerodynamics; Settles 2005) and transport of inspired scent within the nasal cavity
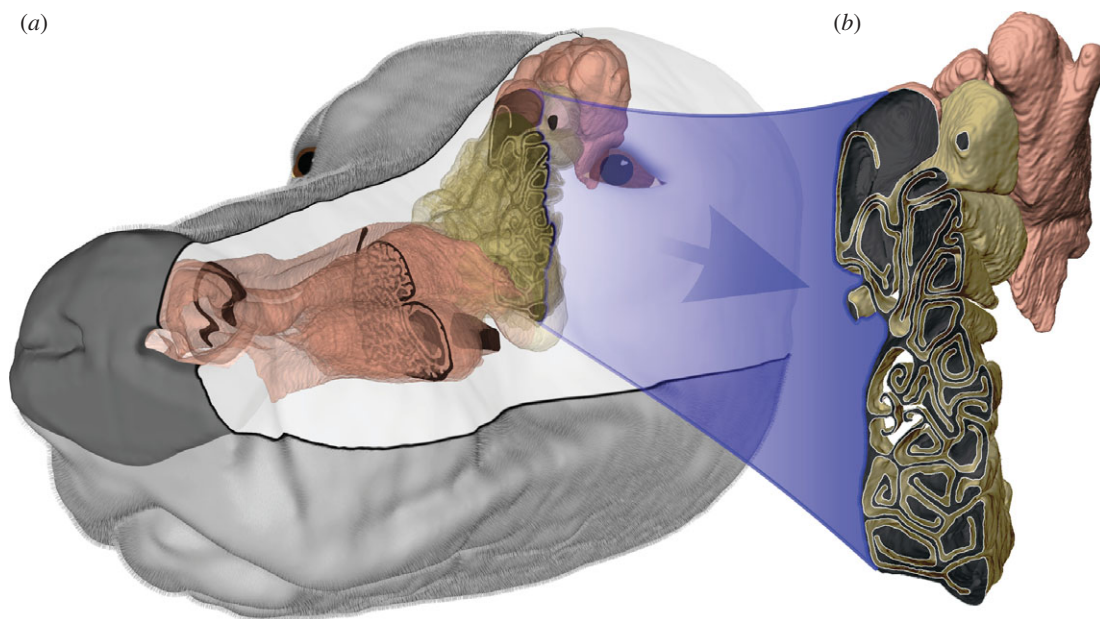
*Author for correspondence (craven@psu.edu).

(a) (b)

Figure 1. The canine nasal airway. (*a*) Three-dimensional model of the left canine nasal airway, reconstructed from high-resolution MRI scans. (*b*) The olfactory recess is located in the rear of the nasal cavity and contains scroll-like ethmoturbinates, which are lined with olfactory epithelium. The olfactory (yellowish-brown) and respiratory (pink) regions shown here correspond to the approximate locations of sensory (olfactory) and non-sensory (squamous, transitional and respiratory) epithelium, respectively (Craven *et al.* 2007).

(intranasal fluid dynamics). These phenomena provide bilateral samples of the odour environment for some animals (Wilson & Sullivan 1999; Rajan *et al.* 2006; Porter *et al.* 2007) and also determine the eventual fate of inspired scent since nasal airflow patterns control whether or not odour-laden air reaches the olfactory region of the nose, where odorant detection occurs. However, little is known about the fluid dynamics of olfaction except in rodents (Kimbell *et al.* 1997; Zhao *et al.* 2006; Yang *et al.* 2007) and humans (Hahn *et al.* 1993; Keyhani *et al.* 1995, 1997; Subramaniam *et al.* 1998; Kelly *et al.* 2000; Zhao *et al.* 2004, 2006; Shi *et al.* 2006). How odorant molecules reach the olfactory part of the nasal cavity during sniffing without being filtered by respiratory airways is not well understood, especially in non-primate mammals with extensive filtering apparatuses (Shepherd 2004). Given the convoluted nasal airway of most keen-scented species, particularly the canine (figures 1 and 2*a*; Craven *et al.* 2007), it is hypothesized that such fluid dynamic transport phenomena are highly optimized.

In addition to odorant receptors, a second class of chemosensory receptors was recently discovered in the mouse olfactory epithelium that is apparently associated with the detection of pheromones (Liberles & Buck 2006). Genes that encode these receptors have also been identified in humans and fish (Gloriam *et al.* 2005; Liberles & Buck 2006). Traditionally, pheromone detection in the canine is attributed to receptors in the vomeronasal organ, located in the rostral–ventral part of the nasal cavity (Evans 1993). However, given the discovery of Liberles & Buck (2006), the dog may also possess pheromone receptors in the sensory epithelium lining the olfactory recess.

In the respiratory airways, members of the bitter taste receptor (T2R) family are expressed in both ciliated and innervated epithelial cells. Shah *et al.* (2009) recently reported that motile cilia in the proximal respiratory airways of the human are chemosensory, expressing T2R receptors that detect noxious chemicals and initiate a signalling cascade, which leads to an increased ciliary beat frequency for enhanced mucociliary clearance. In rats and mice, Finger *et al.* (2003) located solitary chemoreceptor cells in the nasal respiratory epithelium that synapse with trigeminal afferent nerve fibres and express T2R receptors. Thus, in addition to free nerve endings beneath the epithelial surface, trigeminal chemosensory cells activate the trigeminal nerve when stimulated by inhaled noxious substances (Finger *et al.* 2003). Similar chemosensory function may also occur by motile cilia and non-olfactory innervated cells in the nasal cavity of the dog (see Evans (1993) for a description of the trigeminal and other cranial nerves).

2. OBJECTIVES

The objective of this study was to investigate canine nasal airflow and the implications regarding olfaction using a combined experimental and computational approach. Time-accurate airflow measurements of canine sniffing are first presented and are used to characterize the airflow rate, tidal volume and frequency of olfactory sampling by the domestic dog. Allometric scaling of the experimental data is demonstrated, which yields unique size-dependent relationships that describe air intake during sniffing. Using these data and a reconstructed anatomically accurate three-dimensional model of the nasal cavity, a high-fidelity computational fluid dynamics (CFD) simulation of sniffing is carried out that is used to study the external and internal fluid dynamics of olfaction in the dog. The functional
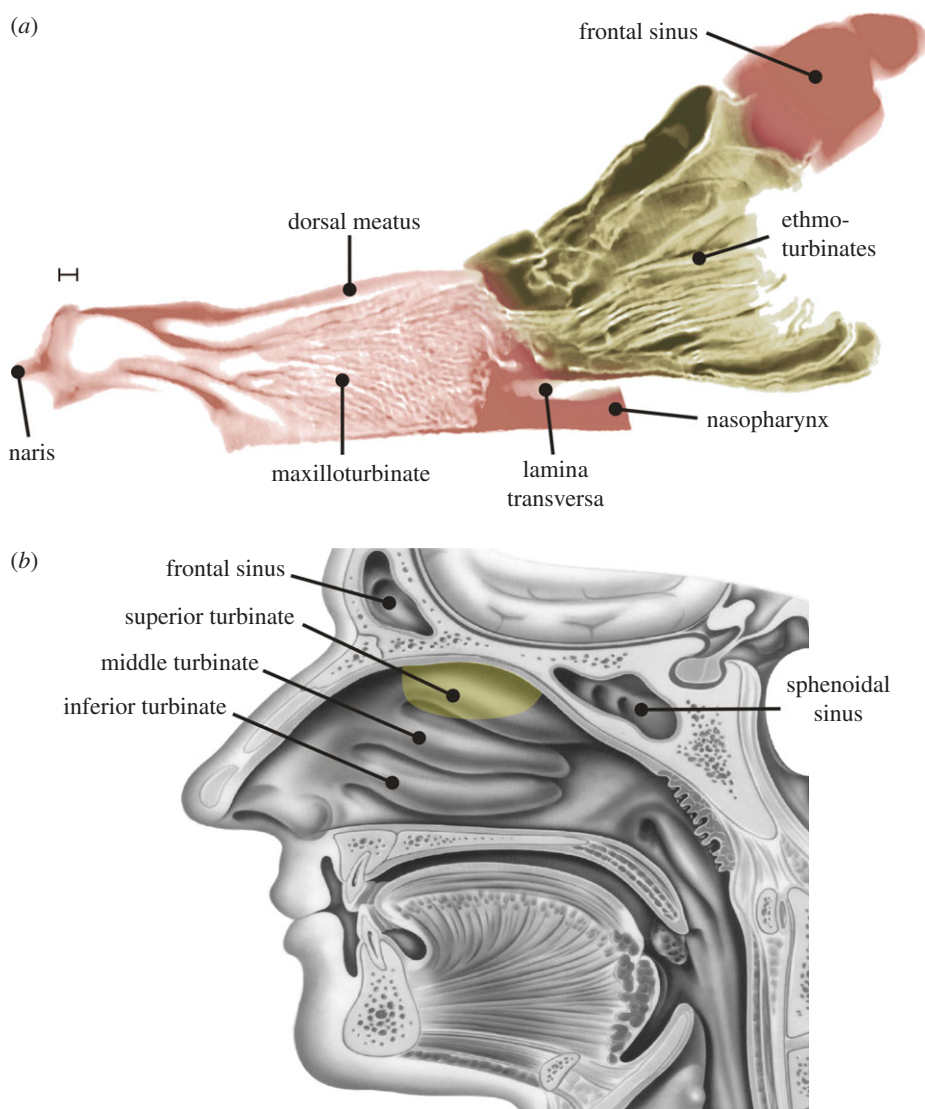
Figure 2. The canine olfactory recess. (*a*) A sagittal section of the canine nasal airway reveals a peripherally located olfactory recess excluded from the respiratory part of the nose by a bony horizontal plate, the *lamina transversa*. This anatomical feature is characteristic of keen-scented (macrosmatic) animals and influences olfactory airflow patterns and odorant transport. Scale bar 2.5 mm. (*b*) For comparison, a sagittal view of the human nasal airway demonstrates the absence of an olfactory recess in the human nose (courtesy Hornung 2006). Here, the delineation of the olfactory region is as illustrated by Lang (1989). As shown by Morrison & Costanzo (1990, 1992), the shift from respiratory to olfactory epithelium is not uniform or well defined, but rather is characterized as having a mixed and irregular boundary, where clusters of olfactory cells are found among non-olfactory cells. The olfactory region shown here corresponds to the approximate location of the olfactory epithelium. Yellowish-brown, olfactory region; pink, respiratory region.

implications of canine nasal airflow regarding olfaction are next considered. Lastly, a discussion and comparison of our results with nasal airflow in other species is provided that yields a new general explanation of mammalian olfactory function based on intranasal airflow patterns generated during sniffing, which partly explains the disparity in olfactory acuity of different animals and the macrosmatic versus microsmatic classification.

3. MATERIAL AND METHODS

3.1. Experimental sniffing measurements

To characterize canine sniffing, seven dogs, ranging over nearly an order of magnitude in body mass

(6.8–52.9 kg), were conditioned to sniff odour stimuli while wearing a muzzle that was specially designed to measure the time-accurate airflow rate during sniffing. As shown in figure 3, the muzzle design was minimally intrusive and consisted of a hot-film probe centred within the neck of an inlet contraction that included a smoothly contoured inlet 'fairing' (figure 3*a*). A short aerodynamic contraction was used to prevent separated airflow at the inlet during inspiration. Larger muzzle contractions were used in preliminary experiments, but were found to distract the animal subjects and prevented natural sniffing behaviour. Further, a transparent material was selected because the animals, likewise, were distracted by opaque muzzles. A strip of vinyl foam was used to form a seal between the muzzle and the dog's snout (figure 3*a*).
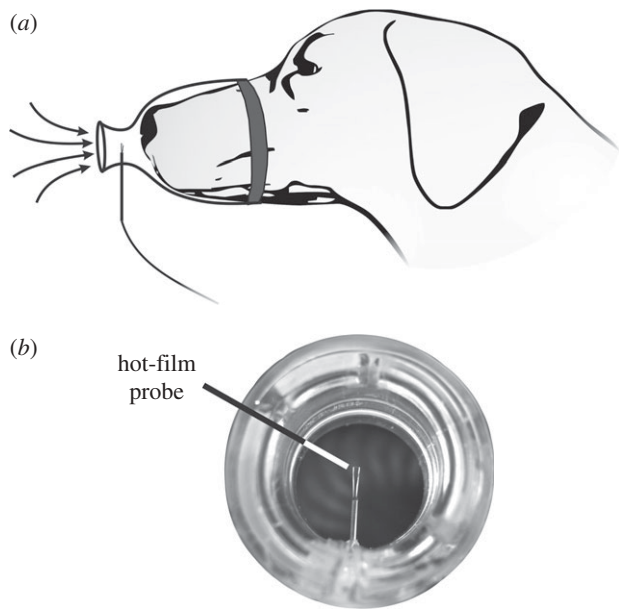
(a)

(b)

hot-film
probe

Figure 3. Experimental measurements of canine sniffing. (*a*) Schematic of the experimental technique. (*b*) A photograph of the inlet to the specially designed muzzle used for time-accurate airflow measurements of canine sniffing.

(a)

insp.

exp.

(b)

(c)

Figure 4. Experimental results from airflow measurements of canine sniffing. (*a*) Sample measurements for three dogs of widely different body size reveal the size-dependent variation of airflow rate for canine sniffing. Here, short sniffing bouts are shown that consist of a single burst of sniffs. (*b*) Longer bouts of sniffing typically contained multiple bursts of sniffs occurring in the 0.5–1.5 Hz range. (*c*) A plot of the normalized power spectral density (PSD) of sniffing calculated via a fast Fourier transform (FFT) of the time-dependent airflow rate data. For comparison, each PSD spectrum is normalized by the maximum PSD. Red lines, Pomeranian (6.8 kg); green lines, sheltie–husky mix (14.5 kg); blue lines, German shepherd (34.5 kg); black lines, Labrador retriever (52.9 kg).

The airflow rate was obtained by calibrating the muzzle against a commercial flow meter (TSI Inc., model 4043). The experimental uncertainty was assessed by considering the error in the measured airflow rate associated with variable ambient air temperature. Given an ambient air temperature range of approximately 19–23°C, from a rigorous uncertainty analysis the overall error in these measurements was shown to be well bounded by ±10 per cent experimental uncertainty.

Each animal was trained to sniff a series of scent sources that were novel and unknown to it, comprising both food and neutral objects (Craven 2008), while wearing the muzzle. When presented with an unknown scent source, each of the dogs showed a curious instinctive response that included olfactory sampling via bouts of sniffing. Since long series of sniffs were desired, odours were presented continuously. In contrast, animals trained via operant techniques for odorant discrimination (Youngentob *et al.* 1987; Uchida & Mainen 2003) or localization (Marshall & Moulton 1977) sample odour with short bouts of sniffing. Our experiments, which were in compliance with protocol number 28431 as approved by the Institutional Animal Care and Use Committee at Penn State University, consisted of much longer bouts.

The present experimental technique permitted accurate measurement of inspiratory airflow rate, but only limited accuracy of expiratory airflow rate measurements. Consequently, quantitative expiratory results are not presented, though the qualitative characteristics are discussed. Nevertheless, compared with similar measurements made using a pneumotachometer (Marshall & Moulton 1977; Youngentob *et al.* 1987), this technique has minimal airflow resistance and thus a minimal influence on natural sniffing behaviour.
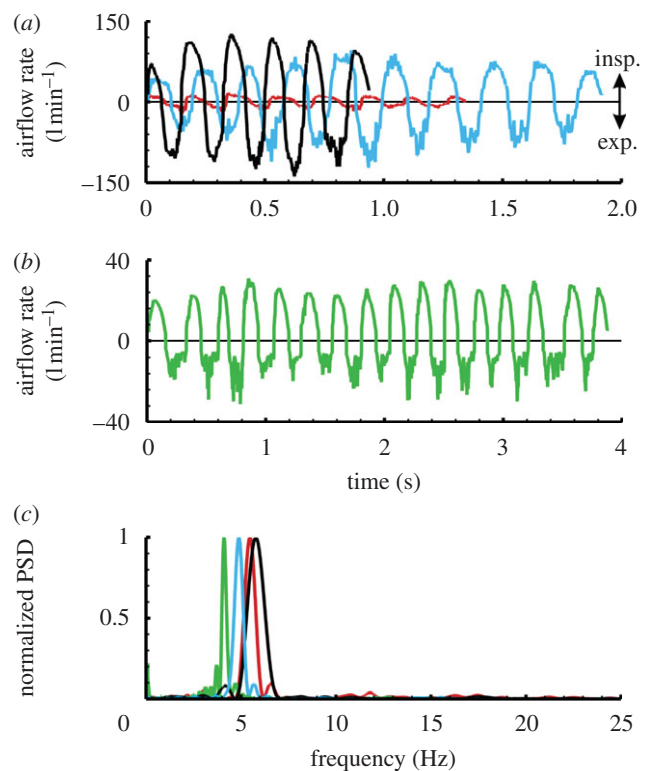
In all of the reported experiments, upon presentation of the scent source, there was an observed shift from respiration to sniffing by each of the dogs that was accompanied by the characteristic nostril motion described by Settles *et al.* (Settles *et al.* 2003; Settles 2005). Quantitatively, the measured response (frequency and airflow rate) was absolutely distinguishable from respiration. Specifically, sniffing occurred at a much higher frequency and yielded significantly higher airflow rates than normal respiration.

In general, inspiratory and expiratory phases of a sniff were easily distinguishable by the degree of unsteadiness in the measurement. Inspiratory measurements were smooth with little unsteadiness owing to the potential flow inlet of the muzzle, whereas expiratory airflow rates exhibited much unsteadiness owing to the turbulent exhaled air jet (figure 4*a*,*b*). The sniff frequency was determined via a fast Fourier transform (FFT) of the time-dependent airflow rate data (figure 4*c*). Consequently, the overall uncertainty in the reported sniff frequencies is low; a conservative estimate is ±1 per cent.

Forty-five trials containing over 300 sniffs were recorded, where for each animal multiple scent stimuli

were tested to measure the natural range in sniff modulation associated with different odorants and concentrations. Though we did not explicitly correlate the results with either variable, some variability in the measurements was observed for the various odour stimuli, much like that briefly described elsewhere for the canine (Marshall & Moulton 1977) and also observed in the rat (Youngentob *et al.* 1987).

3.2. Computational fluid dynamics

An anatomically correct three-dimensional model of the left nasal airway of a 29.5 kg female Labrador retriever mixed-breed canine cadaver, reconstructed from high-resolution magnetic resonance imaging (MRI) scans (Craven *et al.* 2007), was used to carry out a large-scale CFD calculation of incompressible nasal airflow during a 5 Hz sniff. Development and verification of the model, which is generally representative of the mesaticephalic canine nasal cavity (Craven *et al.* 2007), has been shown (Craven *et al.* 2009). Here, we describe the fluid dynamics of canine olfaction from high-fidelity simulation results of physiologically realistic sniffing.

4. RESULTS

4.1. Experimental characterization of canine sniffing

In general, sniffing consisted of an alternating series of inspirations and expirations in a roughly sinusoidal pattern, lasting from about one-half second up to several seconds for a long train of sniffs. Each trial typically contained a single bout of sniffs, while two distinct bouts rarely occurred and three were never observed. A bout, defined here as a period of active sniffing, characteristically began with a relatively weak sniff followed by a crescendo towards the largest sniff, judged by its airflow rate. Though a similar phenomenon has been observed in the rat (Youngentob *et al.* 1987), our data, which include longer bouts, reveal a subsequent reduction in sniff airflow rate (figure 4*a*). Further, long bouts of sniffing lasting more than 2 s reveal multiple maxima in airflow rate occurring at a relatively low frequency, in the 0.5–1.5 Hz range (figure 4*b*). Thus, during continuous stimulus presentation, natural sniffing behaviour appeared to be characterized by a subtle low-frequency modulation of sniff intensity organized as 'bursts' of sniffs, where each burst consisted of a crescendo and a decrescendo in airflow rate and lasted anywhere from about 0.5 to 2 s. Short sniffing bouts appeared as a single burst, whereas long bouts frequently contained multiple bursts.

The frequency of sniffing was rather uniform for all seven animals, regardless of odour source. For all trials, each of the dogs sniffed within a frequency band ranging from 4 to 7 Hz (figure 5*a*), which also encompasses the limited canine sniff frequency data reported elsewhere (Marshall & Moulton 1977; Thesen *et al.* 1993). Thus, canine sniff frequency occurs within the theta frequency band of olfactory neural activity (Lledo *et al.* 2005) (3–12 Hz) and is independent of body size, in contrast to respiratory frequency, which scales allometrically with body mass (Stahl 1967; Schmidt-Nielsen 1984). Remarkably, the sniff frequencies reported here compare well with the canine panting frequency measured by Crawford (1962) (5.33 ± 0.7 Hz), who also determined the natural resonant frequency of the canine respiratory system (5.28 ± 0.3 Hz) and concluded that dogs pant at this frequency to minimize energy expenditure. The canine may also sniff at this frequency, in part for the same reason. Further, canine sniff frequency is comparable to that measured in other keen-scented animals (e.g. rabbit (Glebovskii & Marevskaya 1968), rat (Youngentob *et al.* 1987; Uchida & Mainen 2003; Kepecs *et al.* 2007), and mouse (Wesson *et al.* 2008)), but is an order of magnitude faster than human sniffing, which occurs at only 0.3–0.7 Hz (Hornung *et al.* 2001; Hornung 2006; Porter *et al.* 2007) (figure 5*a*).

Inspiratory airflow rate and tidal volume are strong functions of body size; both scale approximately isometrically (figure 5*b*–*d*). In comparison with available data from other animals, rats also appear to fit these trends, whereas humans sniff at proportionally comparable airflow rates (figure 5*b*,*c*), but inspire significantly more air per sniff for their size (figure 5*d*). Moreover, comparing the allometry of olfaction and respiration, the allometric exponent of inspiratory tidal volume for canine sniffing (figure 5*d*) is similar to the well-established relationship for mammalian respiratory tidal volume (Stahl 1967) (1.04 ± 0.01), whereas inspiratory airflow rate (figure 5*b*,*c*) scales unlike the corresponding respiratory parameter, minute volume (Stahl 1967) (0.80 ± 0.01). Thus, unique biological scaling relationships exist for canine olfaction that regulate air intake in a manner fundamentally distinct from respiration.

Lastly, though we have not correlated expiration data, measured airflow rates were consistently less than or equal to inspiratory values, indicating an apparent accumulation of air in the lungs of the dog while sniffing. This behaviour, which has been briefly reported elsewhere (Marshall & Moulton 1977), also occurs in the rat (Youngentob *et al.* 1987).

4.2. External fluid dynamics of canine olfaction

Using the three-dimensional reconstructed model of the canine nasal cavity (figure 1; Craven *et al.* 2007, 2009) and the foregoing experimental data as boundary conditions, a high-fidelity CFD simulation was performed to study the external and internal fluid dynamics of canine olfaction throughout the course of a sniff. The results reveal that, during inspiration, air in the immediate vicinity of the canine nostril is drawn towards the naris, inducing inspiratory airflow within a small hemispherical region ahead of the naris (figure 6*a*). The spatial extent of this region is known as the 'reach' of the nostril. At peak inspiration a nostril reach of approximately 1 cm is induced, which corresponds to the distance within which dogs have been observed to hold their noses from the ground during scent tracking (Thesen *et al.* 1993). Further, the reach of a nostril is smaller than the internostril separation, indicating that each nostril samples air from spatially
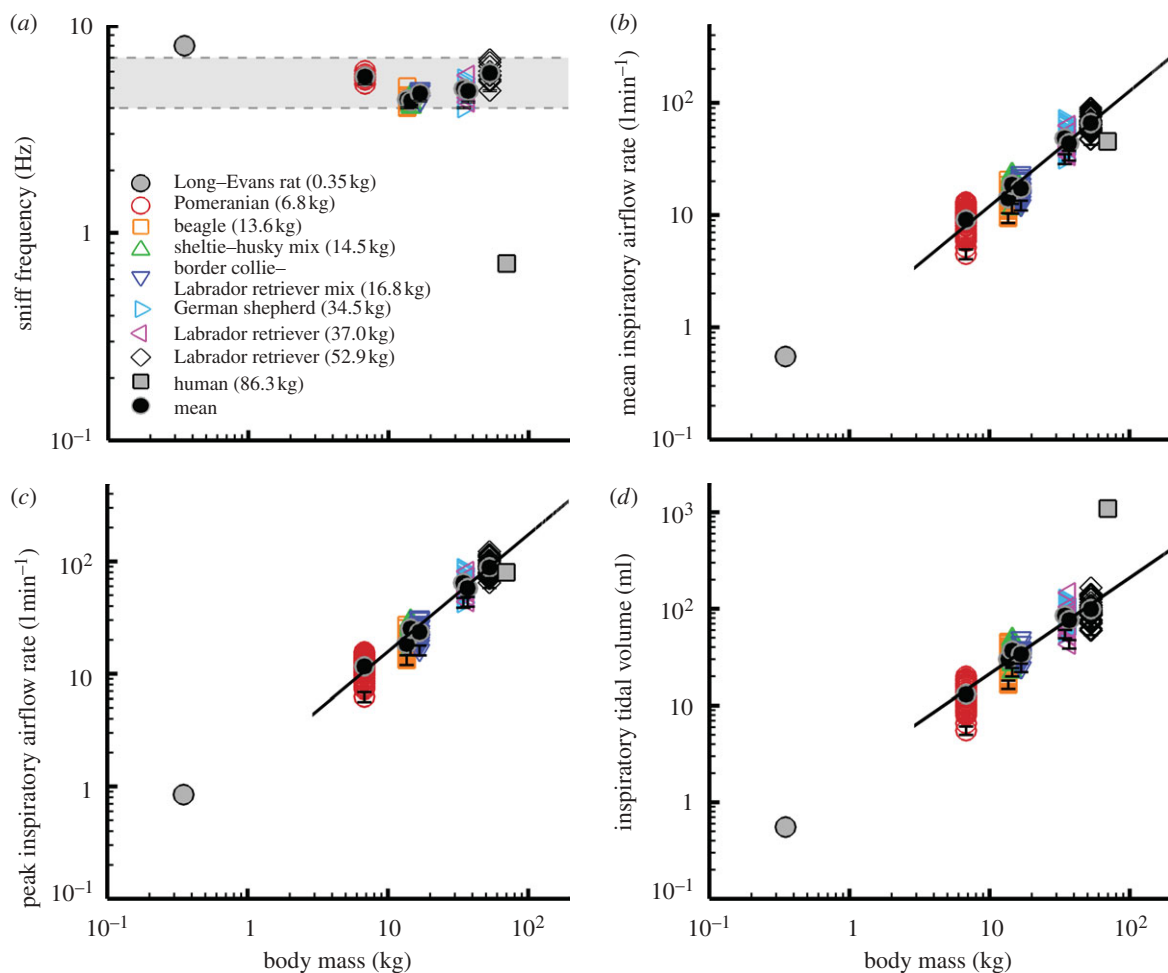
Figure 5. Scaling of the airflow variables of canine sniffing extracted from the time-dependent experimental data. (*a*) Frequency, (*b*) mean inspiratory airflow rate, (*c*) peak inspiratory airflow rate and (*d*) inspiratory tidal volume of canine sniffing versus body mass. (*b–d*) Scaling relationships, calculated as linear regressions of the log-transformed data, include the 95% confidence interval of the allometric exponents. Error bars represent (*a*) $\pm 1\%$ and (*b–d*) $\pm 10\%$ experimental uncertainty. Variability in the flow rate and tidal volume data is attributable to the observed rhythmic modulation of sniff airflow rate within a burst of sniffs and to the range of sniff intensities measured in response to multiple scent sources and variable odour concentration. Mean values for the rat (Youngentob *et al.* 1987; Charles River Laboratories 2009) and human (Vanderburgh *et al.* 1995; Hornung *et al.* 2001; Hornung 2006) are included for comparison. (*b*) $Q_{\text{insp.}}^{\text{mean}} = 1.13 M^{1.03 \pm 0.03}$, $r^2 = 0.92$; (*c*) $Q_{\text{insp.}}^{\text{peak}} = 1.43 M^{1.04 \pm 0.03}$, $r^2 = 0.93$; (*d*) $\forall_{\text{insp.}} = 2.15 M^{0.99 \pm 0.04}$, $r^2 = 0.87$.

separate regions. Thus, the inspiratory external fluid dynamics of canine sniffing yields bilateral odour samples that may be exploited by bilateral neuronal pathways (Rajan *et al.* 2006) and spatially receptive neurons in the piriform cortex (Wilson 1997; Wilson & Sullivan 1999) for odour source localization.

On expiration, owing to the internal shape of the nasal vestibule (Craven *et al.* 2007), a ventral-laterally directed air jet is ejected from the nose (figure 6*b*). When sniffing a surface, such as the ground, the direction of the vectored expired airstream is such that it promotes disturbance and mixing of ambient odorants that may be subsequently inspired, while minimizing sample 'blow-off' directly ahead of the nostril. This has been observed in high-speed flow visualization experiments of canine sniffing (Settles *et al.* 2003; Settles 2005). Further, having been warmed by the respiratory airways, the expired jet may volatilize latent odorant traces on the surface (Settles 2005). Two large co-rotating vortices exist within the expired air jet with a rotation such that, when sniffing a surface,

laterally located odorant signal is drawn towards the nose for sampling. Taken together, these fluid dynamic features of canine expiration increase the effective reach of the nose, enabling inspiration of otherwise inaccessible odours.

4.3. Intranasal fluid dynamics of canine olfaction

The internal fluid dynamics of olfaction in the dog is complicated by the compact, multipurpose design of the nasal cavity, where chemical sensing and respiratory air conditioning both occur. Computational solutions of inspiratory airflow during sniffing show that, although combined within the same organ, olfactory and respiratory airflows are fundamentally separate phenomena, each with a distinct flow path through the nasal cavity (figure 7*a*). During inspiration, one airway (the dorsal meatus; figure 2*a*) transports odorant-laden air to the olfactory part of the nose, while respiratory airways direct the remaining airflow away from the
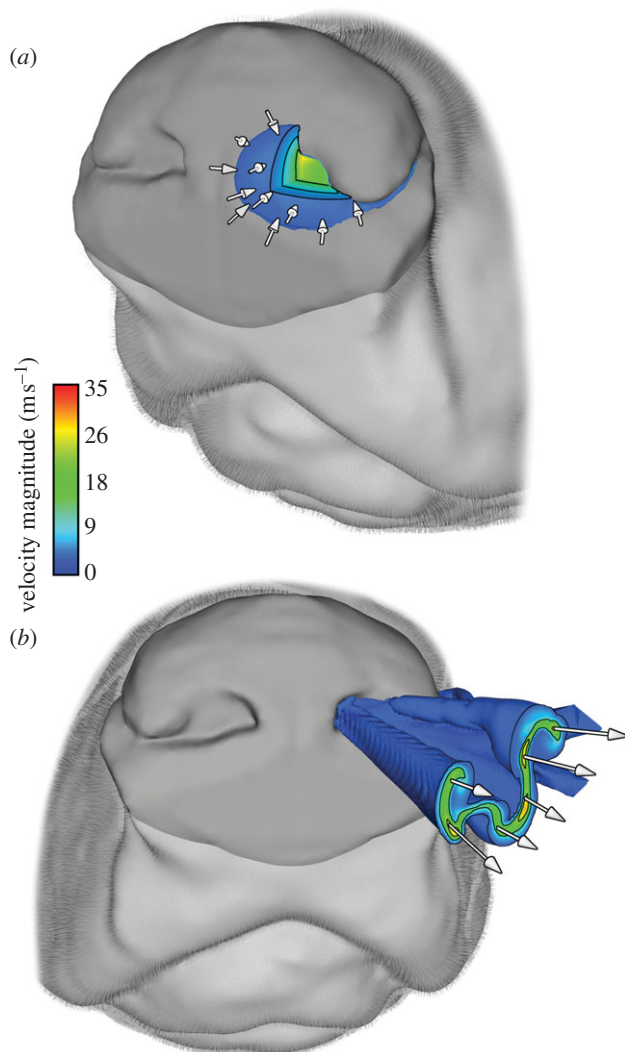
Figure 6. The external fluid dynamics of canine olfaction. (*a*) At peak inspiration, an isosurface of velocity magnitude (10% of maximum inspiratory velocity) reveals the aerodynamic reach of the left nostril, which is approximately 1 cm and smaller than the internostril separation. This airflow pattern provides bilateral odour samples that may be used by the dog for odour source localization. (*b*) At peak expiration, an isosurface of velocity magnitude (10% of maximum expiratory velocity) shows a ventral-laterally directed air jet containing two large co-rotating vortices expelled from the canine nose, which augments odorant collection.

olfactory recess, towards the nasopharynx where it exits the nasal cavity. For the case described here of a relaxed, undilated nostril, the splitting of olfactory and respiratory airflow is such that approximately 12–13% of inspired air reaches the chemosensory region. Including physiologically realistic nostril motion during sniffing, which has yet to be fully defined for the canine, may increase this percentage as shown in CFD solutions of steady inspiration in the rat (Kimbell *et al.* 1997), where an artificial nasal vestibule repositioning to account for nostril mobility resulted in slightly more airflow (approx. 2–3%) reaching the olfactory recess and no change in the overall nasal airflow pattern (see §5 for canine versus rodent nasal airflow).

Upon entering the nasal cavity, inspiratory airflow is well mixed within the nasal vestibule by turbulence prior to splitting into olfactory and respiratory flow paths, thus ensuring delivery of a representative odour sample to the dorsal meatus (Craven *et al.* 2007, 2009; Craven 2008). High-velocity olfactory airflow in the dorsal meatus then quickly transports the odorant to the rear of the olfactory recess, where the airflow turns 180° and slowly filters forward through the olfactory airway labyrinth (figure 7*b*). Here the small size and intricate scrollwork of the olfactory airways promote laminar flow and provide a large surface area (approx. 200 cm^2) (Craven *et al.* 2007) for odorant deposition. Finally, olfactory airflow either exits the nasal cavity via the nasopharynx or continues to flow forward into the dorsal-most ethmoturbinate extensions of the olfactory recess (Craven *et al.* 2007), where it remains at the conclusion of inspiration (shown in figure 7*a*,*b* as pathlines that terminate in this region).

During expiration, owing to the architecture of the nasal cavity, no appreciable airflow enters or exits the olfactory recess (figure 7*c*); throughout this phase of the sniff, the air in the olfactory region is essentially quiescent. Expiratory airflow proceeds from the nasopharynx, through the respiratory region, and exits the nasal cavity at the naris. Functionally, this unique nasal airflow pattern that develops during sniffing, which includes unidirectional laminar flow through the olfactory recess during inspiration and a quiescent period during expiration, is ideal for 'chromatographic' odorant separation (Mozell 1964; Schoenfeld & Cleland 2005) and provides additional residence time for odorant vapour absorption (Craven 2008), respectively.

5. DISCUSSION

5.1. The role of the canine olfactory recess in olfaction

The anatomical structure of the canine nasal cavity is remarkably well organized for efficient intranasal odorant transport, which may partly explain macrosmia in the dog and other similarly organized animals. The overall location and configuration of the sensory region is shown here to be critical to the intranasal fluid dynamics of canine olfaction, forcing a unique nasal airflow pattern during sniffing that is optimized for odorant delivery to the sensory part of the nose. Specifically, the relegation of olfaction to an olfactory recess, in the rear of the nasal cavity and off the main respiratory passage, forces unidirectional airflow there during inspiration and a stagnant period during expiration. Results from a multi-physics vapour transport and deposition model (Craven 2008) show that this cyclic airflow pattern yields unique spatio-temporal odorant deposition patterns along the olfactory epithelium for different chemicals, which may be used by the canine to enhance olfactory discrimination. Accordingly, differential spatio-temporal deposition patterns across the olfactory epithelium of both left and right nasal cavities, resulting from bilateral odour samples provided by the external fluid dynamics of sniffing, could be used for odour source localization. Therefore, the olfactory acuity of the dog appears to inherently depend on its nasal airway architecture and odorant transport by
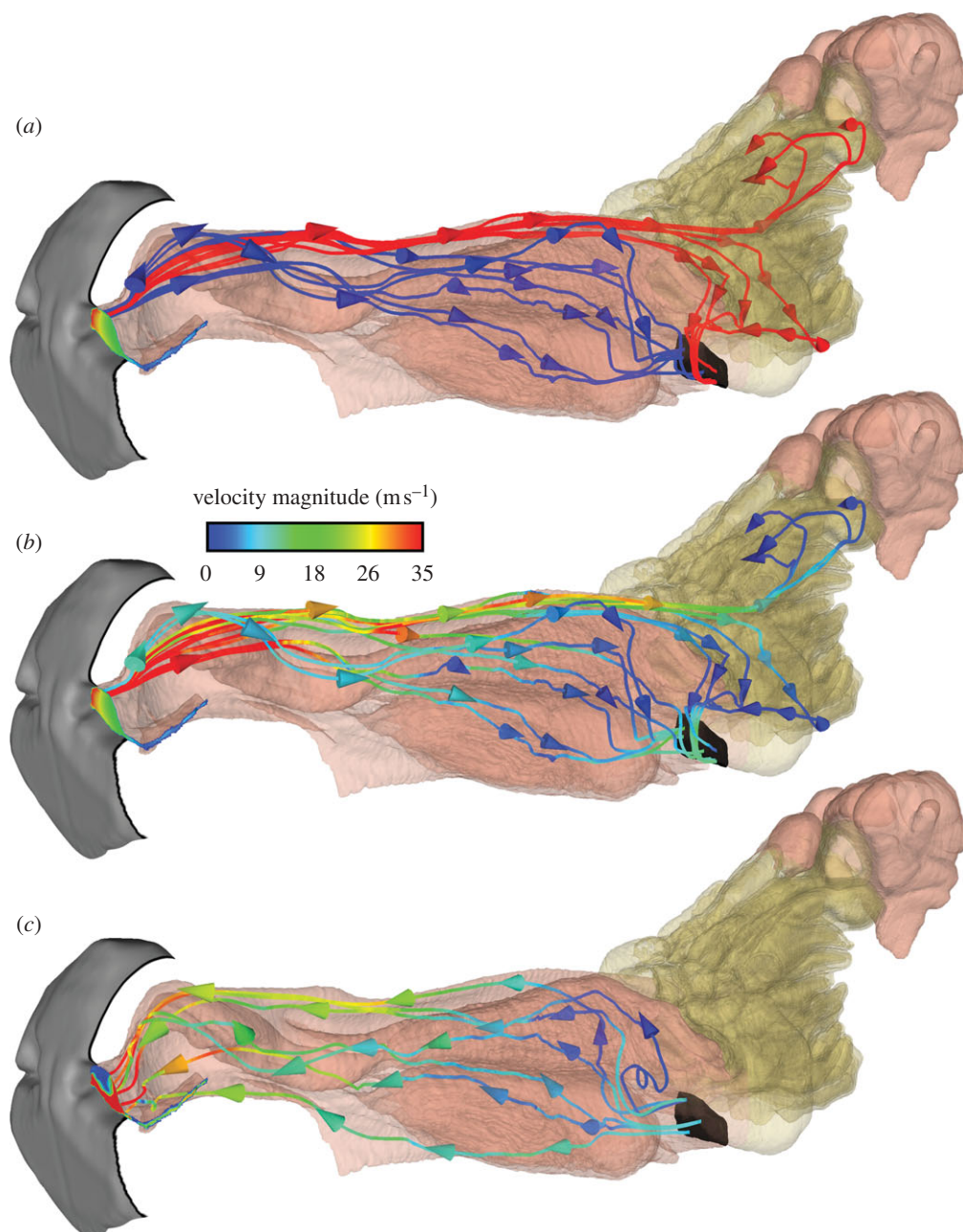
Figure 7. The intranasal fluid dynamics of canine olfaction. (*a*) Unsteady pathlines generated from trajectories of neutrally buoyant particles released from the naris at equally spaced time intervals throughout inspiration reveal distinct respiratory and olfactory flow paths within the nasal cavity. (*b*) The same inspiratory pathlines coloured by velocity magnitude show high-velocity olfactory airflow travelling back through the dorsal meatus and low-velocity airflow filtering through the olfactory recess in the forward–lateral direction. (*c*) Expiratory pathlines originating from the nasopharynx demonstrate that airflow bypasses the olfactory recess during expiration, leaving quiescent scent-laden air there, providing an additional residence time for enhanced odorant absorption. (*a*) Red lines, olfactory pathlines; blue lines, respiratory pathlines.

these unique nasal airflow patterns generated during sniffing.

In general, owing to the nasal cycle (Bojsen-Møller & Fahrenkrug 1971; Webber *et al.* 1987; Sobel *et al.* 1999), *in vivo* airway dimensions will vary periodically depending on the degree of nasal turbinate engorgement (Guilmette *et al.* 1989). Such variability is restricted to the respiratory part of the nose, where plentiful vasculature, capable of considerable constriction or dilation, is found in the lamina propria beneath the respiratory epithelium (Negus 1958). In contrast, the lamina propria below the olfactory epithelium does

not contain a rich vascular network and the thickness of the olfactory mucosa does not change appreciably owing to the nasal cycle (see Negus (1958, fig. 99), for photographs of coronal sections of the domestic cat nose that illustrate the influence of vascular constriction and dilation on nasal airway dimensions in respiratory versus olfactory parts of the nose).

Functionally, the canine nasal cycle periodically changes the airflow resistance of the nose via autonomic nervous control of the respiratory nasal vasculature (Lung & Wang 1989), which may result in a reduction of or increased airflow through either nasal cavity

during sniffing. This may alter the airflow rate and the fraction of inspired air reaching the olfactory recess via the dorsal meatus, but because the olfactory part of the nose does not undergo vascular constriction or dilation, the nasal cycle is not expected to affect the unique nasal airflow patterns reported here during sniffing.

5.2. A general explanation of macrosmia

Considering gross nasal airway anatomy, all macrosmatic species (e.g. carnivores (Van Valkenburgh *et al.* 2004; Craven *et al.* 2007), rodents (Schreider & Raabe 1981), ungulates (Negus 1958) and marsupials (Negus 1958)) apparently possess the traits required for such olfactory airflow phenomena. Specifically, these animals all have a dorsal meatus bypassing respiratory airways of variable complexity (Negus 1958), leading to an olfactory recess. This general macrosmatic nasal airway architecture probably leads to olfactory airflow patterns similar to those shown here for the canine, which appear to be indicative of high olfactory acuity. Steady-state CFD calculations of nasal airflow in the rat (Kimbell *et al.* 1997; Zhao *et al.* 2006; Yang *et al.* 2007), most recently for expiration (Zhao *et al.* 2006; Yang *et al.* 2007), corroborate this theory.

In contrast, the microsmatic human nasal cavity (figure 2b) has no olfactory recess and the resulting airflow patterns vary markedly from those in the canine and rat (e.g. Keyhani *et al.* (1995), Subramaniam *et al.* (1998) and Zhao *et al.* (2004, 2006) for human nasal airflow results). Further, human sniffing can yield dramatically different intranasal airflow patterns in the right and left nasal cavities of the same subject (Zhao *et al.* 2004) or even separated airflow within the olfactory region (Swift & Proctor 1977), a fluid dynamic phenomenon that is undesirable for consistent odorant deposition and chromatographic separation patterns. Since the olfactory region is located along the main airflow path through the nose and not within a highly developed olfactory recess (figure 2), when humans expire the sensory area is either purged of odorant or delivered a fresh odour sample via the retronasal route. The present results show that this does not occur in the canine, where olfactory stimulation by inspired odorant may continue throughout the expiratory phase of a sniff because the overall nasal airflow pattern prevents retronasal access to the olfactory recess. Therefore, mammalian olfactory function and acuity appears to inherently depend on nasal airway anatomy and the intranasal airflow patterns produced by the presence or absence of an olfactory recess. This may further influence natural sniffing behaviour and partly explain the comparative similarity of canine and rat sniffing shown here in contrast to the microsmatic human.

REFERENCES

Bojsen-Møller, F. & Fahrenkrug, J. 1971 Nasal swell-bodies and cyclic changes in the air passage of the rat and rabbit nose. *J. Anat.* **110**, 25–37.

Charles River Laboratories 2009 Long-Evans rats. See http://info.criver.com/flex_content_area/documents/rm_rm_c_long_evans_rats.pdf.

Craven, B. A. 2008. *A fundamental study of the anatomy, aerodynamics, and transport phenomena of canine olfaction.* University Park, PA: The Pennsylvania State University.

Craven, B. A., Neuberger, T., Paterson, E. G., Webb, A. G., Josephson, E. M., Morrison, E. E. & Settles, G. S. 2007 Reconstruction and morphometric analysis of the nasal airway of the dog (*Canis familiaris*) and implications regarding olfactory airflow. *Anat. Rec.* **290**, 1325–1340. (doi:10.1002/ar.20592)

Craven, B. A., Paterson, E. G. & Settles, G. S. 2009 Development and verification of a high-fidelity computational fluid dynamics model of canine nasal airflow. *J. Biomech. Eng.* **131**, 1–11.

Crawford, E. C. 1962 Mechanical aspects of panting in dogs. *J. Appl. Physiol.* **17**, 249–251.

Evans, H. E. 1993 *Miller's anatomy of the dog*, 3rd edn. Philadelphia, PA: Saunders.

Finger, T. E., Bottger, B., Hansen, A., Anderson, K. T., Alimohammadi, H. & Silver, W. L. 2003 Solitary chemoreceptor cells in the nasal cavity serve as sentinels of respiration. *Proc. Natl Acad. Sci. USA* **100**, 8981–8986. (doi:10.1073/pnas.1531172100)

Glebovskii, V. D. & Marevskaya, A. P. 1968 Participation of muscles of the nostrils in olfactory analysis and respiration in rabbits. *Fiziol. Zh.* **54**, 1278–1286.

Gloriam, D. E. I., Bjarnadóttir, T. K., Yan, Y. L., Postlethwait, J. H., Schiöth, H. B. & Fredriksson, R. 2005 The repertoire of trace amine G-protein-coupled receptors: large expansion in zebrafish. *Mol. Phylogenet. Evol.* **35**, 470–482. (doi:10.1016/j.ympev.2004.12.003)

Guilmette, R. A., Wicks, J. D. & Wolff, R. K. 1989 Morphometry of human nasal airways *in vivo* using magnetic resonance imaging. *J. Aerosol. Med.* **2**, 365–377. (doi:10.1089/jam.1989.2.365)

Hahn, I., Scherer, P. W. & Mozell, M. M. 1993 Velocity profiles measured for airflow through a large-scale model of the human nasal cavity. *J. Appl. Physiol.* **75**, 2273–2287.

Hornung, D. E. 2006 Nasal anatomy and the sense of smell. *Adv. Otorhinolaryngol.* **63**, 1–22.

Hornung, D. E., Smith, D. J., Kurtz, D. B., White, T. & Leopold, D. A. 2001 Effect of nasal dilators on nasal structures, sniffing strategies, and olfactory ability. *Rhinology* **39**, 84–87.

Kelly, J. T., Prasad, A. K. & Wexler, A. S. 2000 Detailed flow patterns in the nasal cavity. *J. Appl. Physiol.* **89**, 323–337.

Kepecs, A., Uchida, N. & Mainen, Z. F. 2007 Rapid and precise control of sniffing during olfactory discrimination in rats. *J. Neurophysiol.* **98**, 205–213. (doi:10.1152/jn.00071.2007)

Keyhani, K., Scherer, P. W. & Mozell, M. M. 1995 Numerical simulation of airflow in the human nasal cavity. *J. Biomech. Eng.* **117**, 429–441. (doi:10.1115/1.2794204)

Keyhani, K., Scherer, P. W. & Mozell, M. M. 1997 A numerical model of nasal odorant transport for the analysis of

human olfaction. *J. Theor. Biol.* **186**, 279–301. (doi:10.1006/jtbi.1996.0347)

Kimbell, J. S., Godo, M. N., Gross, E. A., Joyner, D. R., Richardson, R. B. & Morgan, K. T. 1997 Computer simulation of inspiratory airflow in all regions of the F344 rat nasal passages. *Toxicol. Appl. Pharmacol.* **145**, 388–398. (doi:10.1006/taap.1997.8206)

Kuramoto, K., Nishida, T. & Mochizuki, K. 1985 Morphological study on the nasal turbinates (Conchae) of the pika (*Ochotona rufescens rufescens*) and the volcano rabbit (*Romerolagus diazi*). *Anat. Histol. Embryol.* **14**, 332–341.

Lang, J. 1989 *Clinical anatomy of the nose, nasal cavity and paranasal sinuses.* Stuttgart, NY: Thieme.

Liberles, S. D. & Buck, L. B. 2006 A second class of chemosensory receptors in the olfactory epithelium. *Nature* **442**, 645–650. (doi:10.1038/nature05066)

Lledo, P. M., Gheusi, G. & Vincent, J. D. 2005 Information processing in the mammalian olfactory system. *Physiol. Rev.* **85**, 281–317. (doi:10.1152/physrev.00008.2004)

Lung, M. A. & Wang, J. C. C. 1989 Autonomic nervous control of nasal vasculature and air-flow resistance in the anesthetized dog. *J. Physiol. Lond.* **419**, 121–139.

Marshall, D. A. & Moulton, D. G. 1977 Quantification of nasal air flow patterns in dogs performing an odor detection task. In *Proc. Sixth International Symposium on Olfaction and Taste. Olfaction and Taste VI* (eds J. LeMagnen & P. MacLeod), p. 197. Washington, DC: Information Retrieval.

Morrison, E. E. & Costanzo, R. M. 1990 Morphology of the human olfactory epithelium. *J. Comp. Neurol.* **297**, 1–13. (doi:10.1002/cne.902970102)

Morrison, E. E. & Costanzo, R. M. 1992 Morphology of olfactory epithelium in humans and other vertebrates. *Microsc. Res. Tech.* **23**, 49–61. (doi:10.1002/jemt.1070230105)

Mozell, M. M. 1964 Evidence for sorption as a mechanism of olfactory analysis of vapours. *Nature* **203**, 1181–1182. (doi:10.1038/2031181a0)

Negus, V. E. 1958 *The comparative anatomy and physiology of the nose and paranasal sinuses.* London, UK: Livingstone.

Pihstrom, H., Fortelius, M., Hemila, S., Forsman, R. & Reuter, T. 2005 Scaling of mammalian ethmoid bones can predict olfactory organ size and performance. *Proc. Biol. Sci.* **272**, 957–962.

Porter, J., Craven, B., Khan, R. M., Chang, S. J., Kang, I., Judkewicz, B., Volpe, J., Settles, G. & Sobel, N. 2007 Mechanisms of scent-tracking in humans. *Nat. Neurosci.* **10**, 27–29. (doi:10.1038/nn1819)

Proctor, D. F. 1982 The upper airway. In *The nose: upper airway physiology and the atmospheric environment* (eds D. F. Proctor & I. B. Anderson), pp. 23–43. New York, NY: Elsevier Biomedical Press.

Quignon, P. *et al.* 2003 Comparison of the canine and human olfactory receptor gene repertoires. *Genome Biol.* **4**, R80. (doi:10.1186/gb-2003-4-12-r80)

Rajan, R., Clement, J. P. & Bhalla, U. S. 2006 Rats smell in stereo. *Science* **311**, 666–670. (doi:10.1126/science.1122096)

Rouquier, S. & Giorgi, D. 2007 Olfactory receptor gene repertoires in mammals. *Mutat. Res.* **616**, 95–102.

Rouquier, S., Taviaux, S., Trask, B. J., Brand-Arpon, V., van den Engh, G., Demaille, J. & Giorgi, D. 1998 Distribution of olfactory receptor genes in the human genome. *Nat. Genet.* **18**, 243–250. (doi:10.1038/ng0398-243)

Rouquier, S., Blancher, A. & Giorgi, D. 2000 The olfactory receptor gene repertoire in primates and mouse: evidence for reduction of the functional fraction in primates. *Proc. Natl Acad. Sci. USA* **97**, 2870–2874. (doi:10.1073/pnas.040580197)

Schmidt-Nielsen, K. 1984 *Scaling: why is animal size so important?* New York, NY: Cambridge University Press.

Schoenfeld, T. A. & Cleland, T. A. 2005 The anatomical logic of smell. *Trends Neurosci.* **28**, 620–627. (doi:10.1016/j.tins.2005.09.005)

Schreider, J. P. & Raabe, O. G. 1981 Anatomy of the nasalpharyngeal airway of experimental animals. *Anat. Rec.* **200**, 195–205. (doi:10.1002/ar.1092000208)

Settles, G. S. 2005 Sniffers: Fluid-dynamic sampling for olfactory trace detection in nature and homeland security—the 2004 Freeman Scholar Lecture. *J. Fluids Eng.* **127**, 189–218. (doi:10.1115/1.1891146)

Settles, G. S., Kester, D. A. & Dodson-Dreibelbis, L. J. 2003 The external aerodynamics of canine olfaction. In *Sensors and sensing in biology and engineering* (eds F. G. Barth, J. A. C. Humphrey & T. W. Secomb), pp. 323–335. New York, NY: Springer.

Shah, A. S., Ben-Shahar, Y., Moninger, T. O., Kline, J. N. & Welsh, M. J. 2009 Motile cilia of human airway epithelia are chemosensory. *Science* **325**, 1131–1134. (doi:10.1126/science.1173869)

Shepherd, G. M. 2004 The human sense of smell: are we better than we think? *PLoS Biol.* **2**, 572–575.

Shi, H., Kleinstreuer, C. & Zhang, Z. 2006 Laminar airflow and nanoparticle or vapor deposition in a human nasal cavity model. *J. Biomech. Eng.* **128**, 697–706. (doi:10.1115/1.2244574)

Smith, T. D., Bhatnagar, K. P., Tuladhar, P. & Burrows, A. M. 2004 Distribution of olfactory epithelium in the primate nasal cavity: are microsmia and macrosmia valid morphological concepts? *Anat. Rec.* **281A**, 1173–1181. (doi:10.1002/ar.a.20122)

Smith, T. D., Rossie, J. B. & Bhatnagar, K. P. 2007 Evolution of the nose and nasal skeleton in primates. *Evol. Anthropol. Issues News Rev.* **16**, 132–146.

Sobel, N., Khan, R. M., Saltman, A., Sullivan, E. V. & Gabrieli, J. D. E. 1999 Olfaction—the world smells different to each nostril. *Nature* **402**, 35. (doi:10.1038/46944)

Stahl, W. R. 1967 Scaling of respiratory variables in mammals. *J. Appl. Physiol.* **22**, 453–460.

Subramaniam, R. P., Richardson, R. B., Morgan, K. T., Kimbell, J. S. & Guilmette, R. A. 1998 Computational fluid dynamics simulations of inspiratory airflow in the human nose and nasopharynx. *Inhal. Toxicol.* **10**, 473–502.

Swift, D. L. & Proctor, D. F. 1977 Access of air to the respiratory tract. In *Respiratory defense mechanisms* (eds J. D. Brain, D. F. Proctor & L. M. Reid), pp. 63–93. New York, NY: Marcel Dekker, Inc.

Thesen, A., Steen, J. B. & Doving, K. B. 1993 Behaviour of dogs during olfactory tracking. *J. Exp. Biol.* **180**, 247–251.

Uchida, N. & Mainen, Z. F. 2003 Speed and accuracy of olfactory discrimination in the rat. *Nature Neurosci.* **6**, 1224–1229. (doi:10.1038/nn1142)

Vanderburgh, P. M., Mahar, M. T. & Chou, C. H. 1995 Allometric scaling of grip strength by body mass in college-age men and women. *Res. Q. Exerc. Sport* **66**, 80–84.

Van Valkenburgh, B., Theodor, J., Friscia, A., Pollack, A. & Rowe, T. 2004 Respiratory turbinates of canids and felids: a quantitative comparison. *J. Zool.* **264**, 281–293. (doi:10.1017/S0952836904005771)

Walker, D. B., Walker, J. C., Cavnar, P. J., Taylor, J. L., Pickel, D. H., Hall, S. B. & Suarez, J. C. 2006 Naturalistic quantification of canine olfactory sensitivity. *Appl. Anim. Behav. Sci.* **97**, 241–254. (doi:10.1016/j.applanim.2005.07.009)

Walker, J. C., Hall, S. B., Walker, D. B., Kendal-Reed, M. S., Hood, A. F. & Niu, X. F. 2003 Human odor detectability:

new methodology used to determine threshold and variation. *Chem. Senses* **28**, 817–826. (doi:10.1093/chemse/bjg075)

Webber, R. L., Jeffcoat, M. K., Harman, J. T. & Ruttimann, U. E. 1987 MR Demonstration of the nasal cycle in the Beagle dog. *J. Comput. Assist. Tomogr.* **11**, 869–871.

Wesson, D. W., Donahou, T. N., Johnson, M. O. & Wachowiak, M. 2008 Sniffing behavior of mice during performance in odor-guided tasks. *Chem. Senses* **33**, 581–596.

Wilson, D. A. 1997 Binaral interactions in the rat piriform cortex. *J. Neurophysiol.* **78**, 160–169.

Wilson, D. A. & Sullivan, R. M. 1999 Respiratory airflow pattern at the rat's snout and an hypothesis regarding its role in olfaction. *Physiol. Behav.* **66**, 41–44. (doi:10.1016/S0031-9384(98)00269-8)

Yang, G. C., Scherer, P. W. & Mozell, M. M. 2007 Modeling inspiratory and expiratory steady-state velocity fields in the Sprague–Dawley rat nasal cavity. *Chem. Senses* **32**, 215–223. (doi:10.1093/chemse/bjl047)

Youngentob, S. L., Mozell, M. M., Sheehe, P. R. & Hornung, D. E. 1987 A quantitative-analysis of sniffing strategies in rats performing odor detection tasks. *Physiol. Behav.* **41**, 59–69. (doi:10.1016/0031-9384(87)90131-4)

Zhao, K., Scherer, P. W., Hajiloo, S. A. & Dalton, P. 2004 Effect of anatomy on human nasal air flow and odorant transport patterns: implications for olfaction. *Chem. Senses* **29**, 365–379. (doi:10.1093/chemse/bjh033)

Zhao, K., Dalton, P., Yang, G. C. & Scherer, P. W. 2006 Numerical modeling of turbulent and laminar airflow and odorant transport during sniffing in the human and rat nose. *Chem. Senses* **31**, 107–118. (doi:10.1093/chemse/bjj008)